No fitness cost entailed by type VI secretion system synthesis, assembly, contraction, or disassembly in enteroaggregative Escherichia coli

Boris Taillefer, Julien F Giraud, Eric Cascales

Journal of Bacteriology

Bacteriology | Full-Length Text

No fitness cost entailed by type VI secretion system synthesis, assembly, contraction, or disassembly in enteroaggregative *Escherichia coli*

Boris Taillefer,[1] Julien F. Giraud,[1] Eric Cascales[1]

AUTHOR AFFILIATION See affiliation list on p. 10.

ABSTRACT Polymicrobial communities are shaped by beneficial and antagonistic interactions between the different species. One of the key players for competition is the type VI secretion system, a large multiprotein complex that assembles a contractile tail-like structure spanning the entire cytoplasm. This contractile tail is comprised of an inner tube tipped by a puncturing complex and wrapped by a sheath that polymerizes under an extended conformation. Contraction of the sheath propels the needle-like tube complex toward the target cell where it delivers effectors. The ClpV AAA^+ ATPase is then recruited to the contracted sheath and uses the energy of ATP hydrolysis for its disassembly. Due to the size of the apparatus and its mechanism of disassembly, it is thought that the T6SS mechanism of action is costly for the cell, and hence can significantly impact its fitness. By using enteroaggregative *Escherichia coli* strains in which the T6SS is arrested at different stages of its mechanism of action, we show here that there is no significant cost associated with T6SS synthesis, assembly, contraction, or disassembly *in vitro*.

IMPORTANCE Bacteria use weapons to deliver effectors into target cells. One of these weapons, the type VI secretion system (T6SS), assembles a contractile tail acting as a spring to propel a toxin-loaded needle. Due to its size and mechanism of action, the T6SS was intuitively thought to be energetically costly. Here, using a combination of mutants and growth measurements in liquid medium, on plates, and in competition experiments, we show that the T6SS does not entail a growth cost to enteroaggregative *Escherichia coli*.

KEYWORDS growth, cost, energy, ATP, protein transport, secretion system, contraction, toxin delivery, bacterial competition

Bacteria do not live alone but rather form mixed communities in which they may deploy cooperative or aggressive behaviors/strategies (1–3). Competition occurs in all environments but is better studied in the case of pathogenesis, where the resident microbiota of the host competes with invading pathogens, a phenomenon known as colonization resistance (4–6). However, pathogens evolved mechanisms to overcome colonization resistance and to establish themselves in the desired environment (7). Bacterial competition can result from exploitation or interference. While the exploitation strategy is based on the exclusion of bacterial rivals from resource availability, the interference strategy relies on a direct growth inhibition of competitors, notably through the action of antimicrobial molecules (8, 9). Interference competition depends on contact-dependent or -independent mechanisms. Contact-independent competition does not require contact between the two competitor cells but rather acts at distance by secreting soluble and diffusible molecules, peptides, or proteins, such as

Editor George O'Toole, Geisel School of Medicine at Dartmouth, Hanover, New Hampshire, USA

Address correspondence to Eric Cascales, cascales@imm.cnrs.fr.

The authors declare no conflict of interest.

Received 26 October 2023
Accepted 27 October 2023

Published 16 November 2023

antibiotics, polyketides, lantibiotics, or bacteriocins (10–12). In contrast, contact-dependent mechanisms need intimate and sometimes prolonged contact between the attacker cell and its target to transfer antimicrobials. Delivery of these antimicrobials (usually proteinaceous toxins) requires dedicated machineries such as the type IV (T4SS), type 5b (T5bSS), type VI (T6SS), and type VII (T7SS) secretion systems (13–18). The synthesis, biogenesis, and mechanism of action of these machineries can be energetically costly and may constitute an obstacle to efficient competition. An energetic cost has been proposed in the case of the T6SS, which assembles a long structure that spans the entire cell body width (19–21). The T6SS belongs to the broad family of contractile injection systems that use a spring-like mechanism to propel an effector-loaded needle toward target cells (22–25). The T6SS is widespread in Gram-negative bacteria and notably in Pseudomonadata and Bacteroidata (26–28). The T6SS is comprised of two main complexes: the membrane complex (MC) and the phage-like tail contractile structure. In most Pseudomonadata, the MC)is constituted of the TssJ-L-M proteins in a 15:10:10 stoichiometry that assembles a cell envelope-spanning channel-like structure (29–32). This MC serves as a docking station for the tail (33–35). The tail is constituted of the baseplate (BP), the assembly platform for the tubular contractile tube/sheath structure. The BP is composed of six wedges comprised of TssEFGK of 1:2:1:6 stoichiometry, arranged around the trimeric VgrG spike that is sharpened by PAAR (36–39). The tail tube/sheath complex is composed of the inner tube made of stacked Hcp hexameric rings wrapped by the sheath made of TssBC complexes (19). The tail tube/sheath complex, which requires ~720 copies of each tube and sheath protein in enteroaggregative *Escherichia coli* (EAEC), is assembled into a metastable extended conformation that stores energy for the contraction (20, 25). Contraction of the sheath propels the tube and spike loaded with effectors toward the target cell (19, 20). The strength of the contraction and the sharpness of the deployed spike are thought to puncture the target cell membrane to directly deliver the effectors inside the target (20, 24). After contraction, the contracted sheath recruits the ClpV ATPase, which uses ATP to disaggregate and disassemble sheath subunits (40–42). Due to its large number of subunits (the T6SS is assembled from about 2,300 polypeptides), its large structure spanning the cytoplasm, and its ATP-dependent disassembly, it has been proposed that the T6SS is energetically costly (20, 43, 44). Indeed, a recent work showed that the *Campylobacter jejuni* T6SS activity induces a cost in environmental stress conditions that can result in the extinction of T6SS$^+$ cells (45). However, recent studies showed that it is unlikely the case in *Bacteroides fragilis*, *Vibrio cholerae,* and *V. fischerii* (46–48). Here, using strains in which the T6SS is arrested at different stages of its mechanism of action, we show that there is no significant cost associated with T6SS synthesis, assembly, contraction, or disassembly in EAEC.

RESULTS

To determine whether the different stages of the T6SS mechanism of action induce a measurable cost, we engineered four different strains from the parental EAEC wild-type (WT) reference strain 17–2 (Fig. 1). Strain Δ*sci1* carries a deletion of the entire T6SS gene cluster and hence does not express nor produce the T6SS. Strain Δ*tssJ* carries a deletion of the *tssJ* gene, which is the penultimate gene of the T6SS cluster in EAEC (Fig. 1A), encoding the first protein to be recruited during T6SS biogenesis (31). In addition, TssJ is a minor but essential core-component of the T6SS, with only 15 copies per T6SS (32, 49). This strain, therefore, expresses T6SS genes, produces the T6SS subunits, but is unable to assemble the apparatus. Strain *tssB-N3* carries a 3-codon insertion in the *tssB* gene, yielding a TssB variant protein assembling the sheath under the extended conformation but unable to contract (50, 51). In this strain, the T6SS is expressed, produced, assembled, but the sheath does not contract. Finally, strain Δ*clpV* carries a deletion of the *clpV* gene encoding the AAA$^+$ ATPase responsible for the disassembly of the contracted sheath (40–42, 52–54). In this strain, the T6SS is expressed, produced, assembled but the sheath is not disassembled after contraction. Taken together, these strains may

A

B

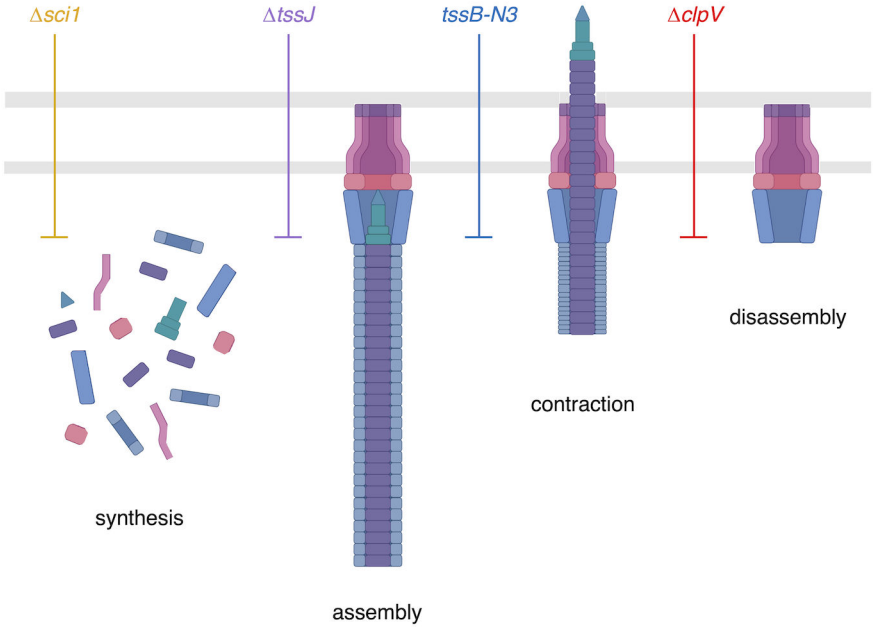

C

strain	expression and production	assembly	contraction	disassembly
WT	+	+	+	+
Δ*clpV*	+	+	+	-
tssB-N3	+	+	-	-
Δ*tssJ*	+	-	-	-
Δ*sci1*	-	-	-	-

FIG 1 EAEC mutant strains used in this work. (A) Schematic representation of the EAEC *sci1* T6SS gene cluster. Genes encoding T6SS subunits and effector/unknown proteins are shown in color and white, respectively. The genes corresponding to the mutants used in this work are indicated. (B) Schematic representation of the different stages of the T6SS mechanism of action: synthesis of the T6SS components, assembly, sheath contraction, and disassembly. The stages in which T6SS biogenesis are arrested in the different mutant strains are indicated. (C) Phenotypes of the indicated strains regarding expression/production, assembly, contraction, and disassembly of the T6SS (– and red highlighting, no; +and green highlighting, yes).

provide information on the cost for T6SS subunit production, T6SS biogenesis, sheath contraction, and disassembly. None of the Δ*tssJ*, *tssB-N3,* and Δ*clpV* strains was impacted in terms of T6SS gene expression and production, as shown by qRT-PCR analyses of *tssK*, *vgrG,* and *tagA* genes (Fig. S1A) and semi-quantitative immunodetection of the Hcp protein (Fig. S1B). All the expected phenotypes of these strains were confirmed by recording sheath number and dynamics after insertion of a fluorescent reporter on

the TssB sheath subunit (Fig. S2). The fluorescence signal was diffuse in the Δ*tssJ* strain, whereas contraction and disassembly of the sheaths were abolished in *tssB-N3* and Δ*clpV* cells, respectively (Fig. S2).

We first measured the generation times of the different strains cultivated at 37°C in SIM medium, a synthetic minimal medium with low iron in which the EAEC T6SS is expressed (55). The 15-h growth curves of the different strains were superimposable (Fig. 2A), yielding comparable doubling times (Fig. 2B). This result suggests that the T6SS does not incur a cost to the producing bacteria. However, the SIM medium does not fully recapitulate the physiological conditions found in the colon in terms of the presence of

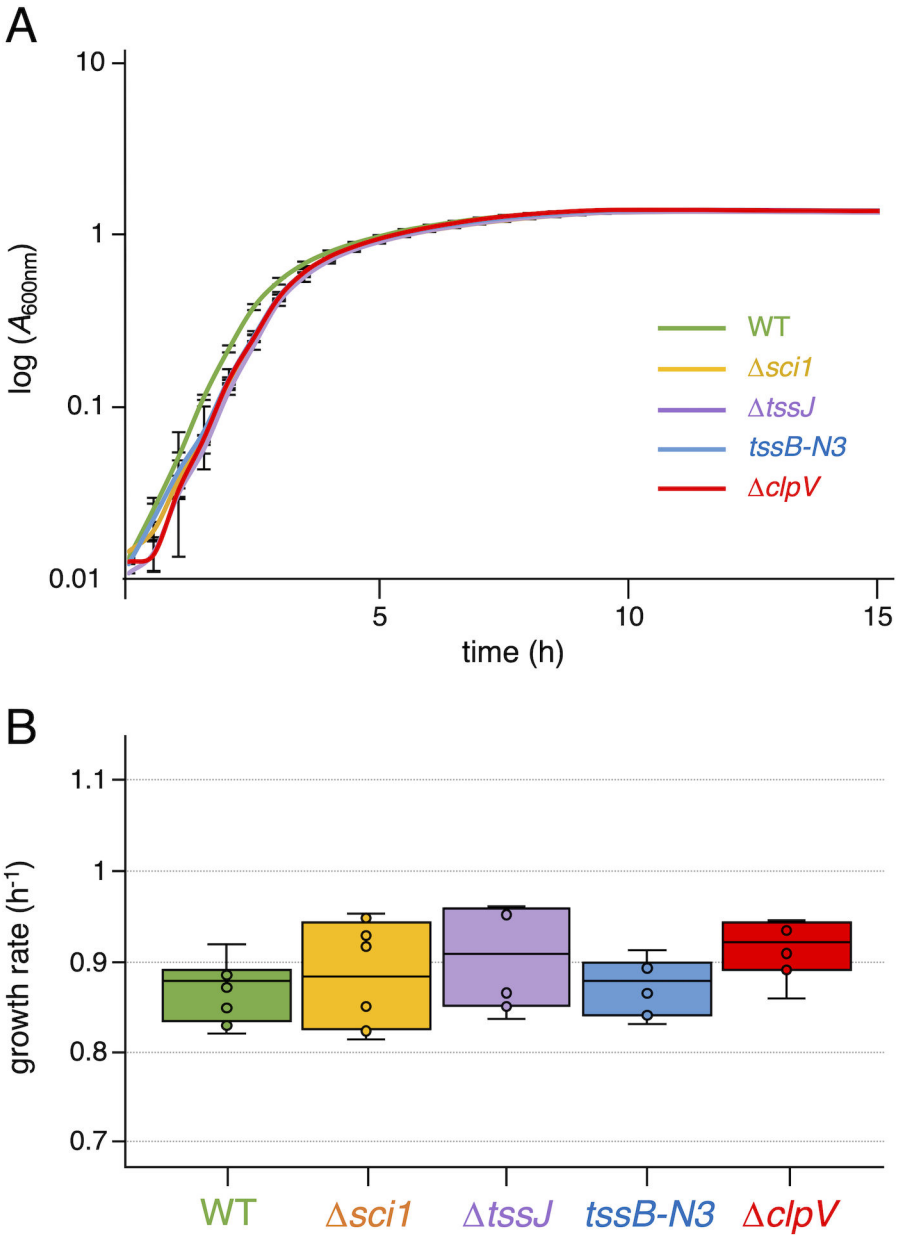

FIG 2 T6SS mutations do not impact growth in liquid culture. (A) 15-h growth curves of the wild-type (WT) strain and the indicated isogenic mutants grown in SIM medium are shown on the same graph. The values represent the average and standard deviation from 12 measures (3 biological replicates, 4 independent measures/replicate). (B) Box-and-whisker representation of the growth rates of the WT strain and its isogenic mutants in SIM medium (horizontal bar, median value; lower and upper boundaries of the box plot, 25% and 75% percentiles, respectively; whiskers, 10%, and 90% percentiles). The independent raw values are shown as circles.

bile salts (0.5%–2%; 56), osmolarity (0.4–1.3 M of sorbitol; 57), oxidative stress (0.1 mM of H_2O_2, 58), or pH (pH 6; 59). No differences between the 17–2 strain and its isogenic Δ*sci1* mutant were also noted when the strains were grown in the presence of 1% of bile salts, 0.8 M of sorbitol, 0.1 mM of H_2O_2, at pH 6, or with a combination of these four stresses (Fig. S3).

However, while produced in these conditions, the EAEC T6SS is not fully activated as it has been established that T6SS is firing on solid conditions (60). We thus repeated the experiments with the same strains grown on solid SIM agar plates. Cell cultures were spotted on filter disks placed on agar. Disks were harvested at regular intervals, cells resuspended in SIM, and the optical density measured at λ = 600 nM. Here again, the growth of the different strains was very similar (Fig. 3A), with no statistical differences (Fig. 3B). It is noteworthy that, as expected, the generation time on solid medium (0.73 h^{-1}) is significantly lower compared to the liquid conditions (0.89 h^{-1}).

To better compare the growth of mutant strains with that of the parental WT strain, a 17–2 strain deleted of the *lacZ* gene was used in *in vitro* challenge experiments. In addition, to avoid intoxication of Δ*sci1* cells by WT cells due to the delivery of the Tle1 toxin encoded within the cluster (61), the Δ*sci1* strain was transformed with a low-copy vector expressing the Tle1 immunity, Tli1. The 17–2 Δ*lacZ* and Δ*sci1* pTli1 strains presented identical growth curves and generation times compared to the WT strain, both in liquid and solid. Indeed, challenge experiments between the WT and the Δ*lacZ* strains demonstrated they grow identically (Fig. 4A) and presented a competitive index of 1.02 ± 0.07 after a 96-h co-culture (Fig. 4B). Co-culture of the Δ*lacZ* strain with the four isogenic T6SS mutants showed a competitive index close to one for all combinations (Δ*sci1* pTli1, 0.99 ± 0.05; Δ*tssJ*, 1.03 ± 0.06; *tssB-N3*, 1 ± 0.04; Δ*clpV* 0.99 ± 0.06) (Fig. 4B), reflecting the observation that the initial ratio between the Δ*lacZ* and the mutant strains did not significantly vary for 96 h (Fig. 4A). Here again, no differences between the 17 and 2 strain and its isogenic Δ*sci1* mutant were observed when the strains were grown in the presence of 1% of bile salts, 0.8 M of sorbitol, 0.1 mM of H_2O_2, at pH 6, or with a combination of these four stresses (Fig. S4). Taken together, these results demonstrate that production, assembly, contraction, and disassembly of the T6SS do not entail a significant fitness cost to EAEC in laboratory conditions in which the T6SS is active, or in conditions mimicking the host environment.

DISCUSSION

By using various mutant strains arrested at different stages of T6SS biogenesis and mechanism of action, we show here that the synthesis, assembly, sheath contraction, and disassembly of the T6SS do not incur a measurable energetic cost to EAEC. This conclusion is similar to what has been recently observed in *Vibrio cholerae* (48) and *Bacteroides fragilis* (46), while another study suggested that no fitness cost is associated with fast-growing exponential-phase *Vibrio fischeri* cells but that the T6SS entails a cost in stationary phase (47). By contrast, it was shown that the growth of *Campylobacter jejuni* $T6SS^+$ cells was significantly impaired compared to that of $T6SS^-$ cells when cultured in the presence of bile salts, a medium that mimics the *in vivo* conditions (45). This could be due to the assembly of the T6SS MC that may alter the envelope permeability barrier, hence increasing the entry of toxic compounds, rather than the cost of the T6SS *per se*. In our conditions, we did not observe any impact of the presence of physiological levels of bile salts, or of osmolarity, oxidative, and pH conditions mimicking the human colon on the growth of EAEC $T6SS^+$ and $T6SS^-$ cells. Nevertheless, all these studies have been performed *in vitro*, and one may expect the *in vivo* conditions to be significantly different. Indeed, in *in vivo* conditions, $T6SS^+$ cells are in contact with other bacterial species, including $T6SS^-$ species, T6SS-resistant strains, and T6SS-armed competitors using a tit-for-tat response, which may lead to a rock/scissor/paper-like dynamics. Using a T6SS could not be advantageous for a bacterium *in vivo* or in the host and may thus depend on the composition of the microbial community or of the ecosystem (46, 62). Several studies have shown that the T6SS provides a significant advantage for colonization in

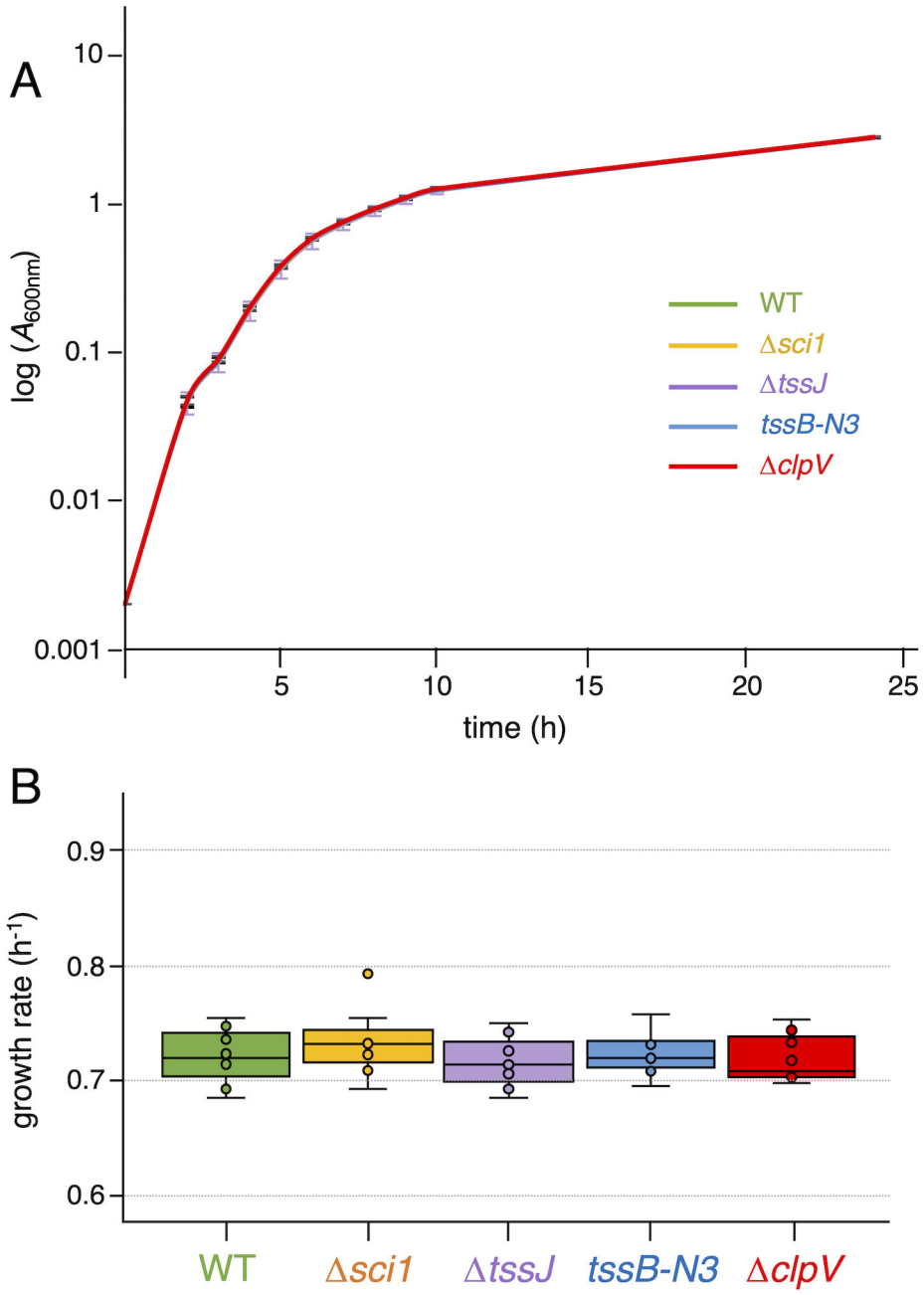

FIG 3 T6SS mutations do not impact growth on solid agar. (A) 24-h growth curves of the wild-type (WT) strain and the indicated isogenic mutants grown on SIM agar plates are shown on the same graph. The values represent the average and standard deviation from nine measures (three biological replicates, three independent measures/replicates). (B) Box-and-whisker representation of the growth rates of the WT strain and its isogenic mutants on SIM agar plates (horizontal bar, median value; lower and upper boundaries of the box plot, 25% and 75% percentiles, respectively; whiskers, 10% and 90% percentiles). The independent raw values are shown as circles.

experimental host models, notably for *Salmonella enterica* Typhimurium, *Shigella sonnei*, *Bacteroides fragilis*, *Vibrio cholerae,* and *Klebsiella pneumoniae* (63–70). However, it is not yet known how the T6SS impacts the persistence in long-term experiments. Robitaille et al. recently showed an evolutionary loss of the T6SS in *B. fragilis in vivo*, suggesting that the T6SS entails a cost in the presence of resistant strains, whereas $T6SS^+$ cells offset the cost paid for T6SS in the presence of sensitive cells (46). By contrast, the presence of T6SS in most Bacteroidota and Pseudomonadata species, particularly those recently isolated,

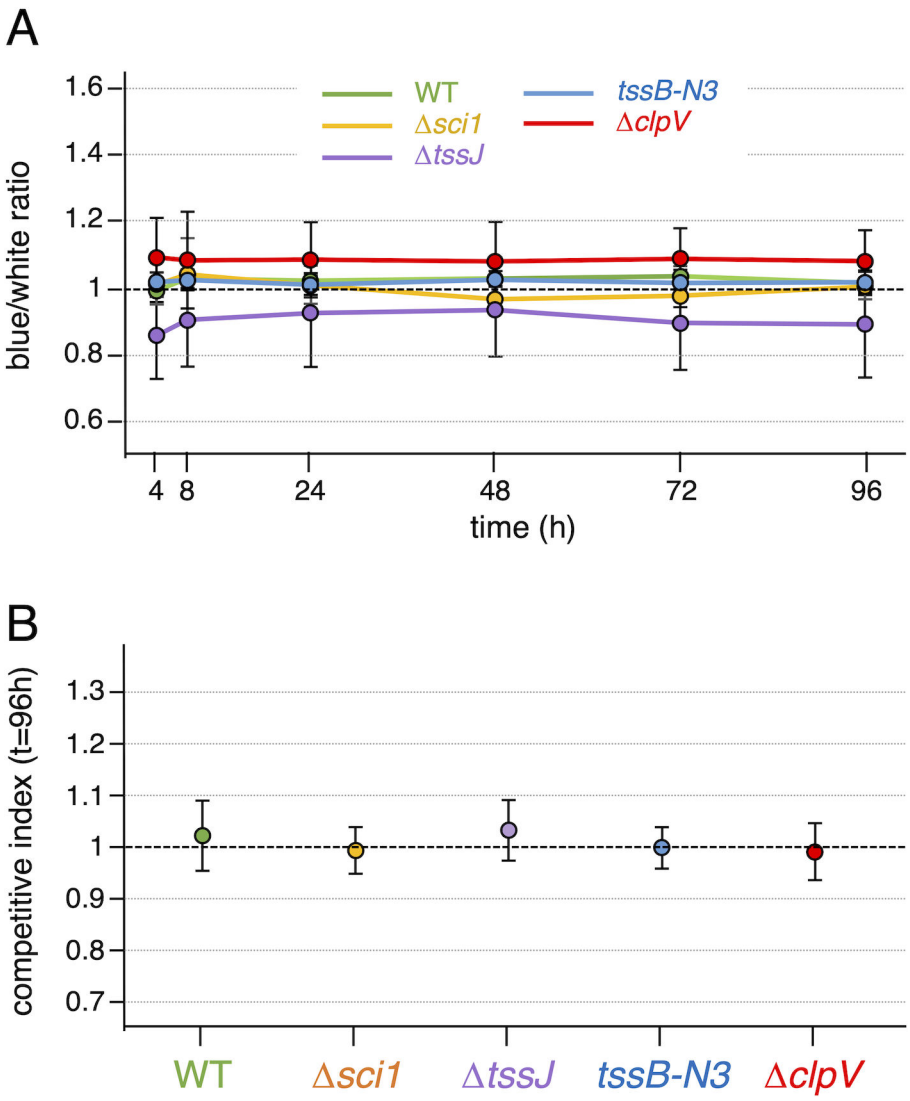

FIG 4 T6SS mutants do not outcompete the wild-type strain. (A) Variation of the ratio of the indicated strain and 17–2Δ*lacZ* over time. The values represent the average and standard deviation from 12 measures (4 biological replicates, 3 independent measures/replicates). (B) Competitive index (indicated strain/Δ*lacZ* ratio after 96 h of co-culture divided by the initial indicated strain/Δ*lacZ* ratio). The values represent the average and standard deviation from 12 measures (4 biological replicates, 3 independent measures/replicate).

suggests that a selective pressure maintains T6SS genes, highlighting its importance in polymicrobial environments.

Given that cryo-tomography and fluorescence microscopy recordings showed that the T6SS assembles a spectacular tail structure that traverses the cytoplasm (19, 21), it was expected to be energetically costly (20, 43, 44). This work and the studies in *Vibrio* and *Bacteroides,* however, contradict this postulate. Indeed, a T6SS with a stoichiometry of $TssJ_{15}$-$TssL_{10}$-$TssM_{10}$-$TssG_{6}$-$TssF_{12}$-$TssE_{6}$-$TssK_{36}$-$VgrG_{3}$-PAAR-Hcp_{720}-$TssB_{720}$-$TssC_{720}$-$TssA_{12}$ represents about 2,300 polypeptides, which is far lower than the 3–10 × 10^{6} estimation for the total number of proteins in a single *E. coli* cell (71), suggesting that synthesis of a T6SS does not have a significant metabolic cost. A rapid calculation of the number of ATP molecules required for synthesis, assembly, and disassembly of a T6SS is also in agreement with the experimental data. Assuming the necessity of five ATP molecules for the addition of one nucleotide during transcription (25 kb T6SS transcript in EAEC) and five ATPs per amino-acid during protein synthesis

(~750,000 amino-acids for a T6SS structure) (72), the synthesis of a T6SS would require ~4 × 10^6 ATPs, while its disassembly (given that ClpXP-mediated denaturation of a substrate requires hydrolysis of ~550 ATPs, 73) would require 750,000 ATPs (20). The cost of synthesis and disassembly of a T6SS structure is therefore in the 10^6–10^7 range, which is, here again, significantly different than the total number of ATP molecules estimated per *E. coli* cell, ~3 × 10^{12} (ATP concentration in *E. coli*: 2.6 mM (74); estimated volume of EAEC cell: 1.8 μm^3). The fact that this secretion system does not entail a significant energetic cost is the opposite to the type III secretion system, whose secretion of translocon proteins and effectors has been shown to cause a significant growth retardation in *Salmonella* Typhimurium (75)

Taken together, our results show that the synthesis, assembly, and disassembly of the T6SS is not energetically costly to enteroaggregative *E. coli* and hence does not incur a significant fitness cost *in vitro*. However, the activity of a T6SS could be costly for the cell in the polymicrobial environment in terms of survival, and notably when in contact with T6SS defensive bacteria that retaliate following an attack.

MATERIALS AND METHODS

Bacterial strains, growth conditions, media, and antibiotics

All strains used in this study are derivatives of the enteroaggregative *E. coli* (EAEC) 17–2 WT strain except the *E. coli* CC118λpir strain, which was used for cloning procedures. Strains Δ*lacZ* (55), Δ*tssJ* (formerly described as Δ*sciN*; 29), TssB-sfGFP (33), and Δ*clpV* (formerly described as Δ*clpV1*; 54) have been already described. *E. coli* cells were routinely grown in Lysogeny Broth (LB). For T6SS expression, EAEC cells were grown at 37°C with agitation in Sci1-inducing medium (SIM; M9 minimal medium supplemented with glycerol 0.25%, vitamin B1 200 $\mu g.mL^{-1}$, casaminoacids 40 $\mu g.mL^{-1}$, $MgCl_2$ 1 mM, $CaCl_2$ 0.1 mM, and LB (10% vol/vol), pH7.1; 55). When required, media were supplemented with kanamycin (50 $\mu g.mL^{-1}$) or chloramphenicol (40 $\mu g.mL^{-1}$). For assays in the presence of different stresses, bile salts (1%, Sigma-Aldrich ref B8756), D-sorbitol (0.8 M, Sigma-Aldrich ref S7547), or H_2O_2 (0.1 mM, Sigma-Aldrich ref H1009) were added in the medium. Commercial anti-His (6His, Proteintech) and anti-EF-Tu (mAb900, Hycult Biotech) monoclonal antibodies were used for immunodetection.

Plasmid and strain construction

Strain 17–2 TssB-N3 bearing an insertion of three residues (AEV) downstream the Gln26 residue at the chromosomal *tssB* locus has been engineered using the suicide vector pKO3-BN3. First, the pKO3-*tssB* vector was engineered by restriction/ligation cloning of a *Sma*I-*Sal*I 1,430 bp DNA fragment encompassing the *tssB* gene into pKO3 (76). This fragment was PCR-amplified using a Biometra thermocycler with the Q5 DNA polymerase (New England Biolabs) and oligonucleotides CACCACCCGGGTTTCCTCAACACTGG and ACGCGTCGACCAGTTGACGGCTGATCTGATAATCAAGCTCTGC (*Sma*I and *Sal*I restriction underlined, respectively). The N3 sequence (GCCGAGGTC, encoding protein sequence AEV) was inserted into pKO3-*tssB* by site-directed mutagenesis using complementary oligonucleotides bearing the desired additional sequence (CCTACATACGGGTGGTGGGC AGGCCGAGGTCAAGAAAGTGGAGCTTCCGCTC and GAGCGGAAGCTCCACTTTCTTGACCTC GGCCTGCCCACCACCCGTATGTAGG, N3 sequence underlined), to yield pKO3-BN3. The pKO3-BN3 plasmid was verified by DNA sequencing (Eurofins) before introduction into strain 17–2 by electroporation. The first and second recombination events were selected on LB plates supplemented with chloramphenicol at 42°C, and supplemented with sucrose (5%), respectively, as previously described (76), to yield strain TssB-N3. Strains Δ*tssJ* TssB-sfGFP, Δ*clpV* TssB-sfGFP, and TssB-N3-sfGFP have been engineered by introducing the sequence encoding the sfGFP to the T6SS native locus on the chromosome, in frame with the *tssB* gene in strains Δ*tssJ*, Δ*clpV,* and TssB-N3, respectively. Chromosomal sfGFP sequence insertion was performed using the one-step inactivation

procedure (77) using λ-red recombination carried by vector pKOBEG (78), by electroporation of a PCR product corresponding to the pKD4-GFP-Cter (33) sfGFP-kanamycin cassette flanked by 50 bp extensions annealing upstream and downstream the last codon of *tssB*. Recombinant strains were selected on LB plates supplemented with kanamycin. All strains were checked by colony-PCR using various oligonucleotide pair combinations, and further verified by DNA sequencing of the PCR amplification of the region of interest.

Quantitative RT-PCR

Total RNAs were extracted from 10^9 cells using the SV Total RNA Isolation kit (Promega), by following the manual instructions. Total RNAs were treated with 1 µL de Turbo DNase for 30 min at 37°C, and the reaction was quenched with the addition of 10 µL of inactivation beads for 10 min. The supernatant, containing the purified total RNAs, was obtained after centrifugation at 10,000 × *g* for 5 min. 500 ng of total RNAs were mixed with oligonucleotide hexamers (Promega) in a final volume of 10 µL and incubated for 5 min at 70°C. After addition of 10 µL of GoScript Reverse Transcriptase, the mixture is incubated for 5 min at 25°C and then for 2 h at 42°C before inactivation for 15 min at 70°C. The cDNAs were then used for quantitative PCR using a Bio-Rad CFX86 Real-Time System. Oligonucleotides used for PCR amplication: 16S RNA (5′-CATGGCTCAGATTGAA CGCTGGCGG and 5′-CGTTATGCGGTATTAGCTACCGTTTCCAG), *tssK* (5′-TAATGGCAGTGAGA GCGAGC and 5′-AACAAGACGGGTAACGGGAC), *vgrG* (5′-GTGGAGCAAATCCTGACGGA and 5′-TCCGGGTGCAACGTAAAGAA), *tagA* (5′-TCAGCAAACTGACTCACCCG and 5′-ACAATCAGA GCCAGCCCTTG).

Growth measurements

Growth measurements in liquid culture

The parental 17–2 (WT) strain and its isogenic Δ*sci1*, Δ*tssJ*, Δ*clpV,* and *tssB-N3* mutant strains were grown overnight in SIM medium (three independent cultures/strain) and diluted to an optical density at λ = 600 nM (A_{600}) of 0.02 in 200 µL of SIM medium (four replicates) disposed in a sterile 96-well suspension culture U-bottom microplate with lid (CellStar 650 185, Greiner Bio-one) and the A_{600} was measured every 30 min for 15 h in a Tecan microplate reader at 37°C, with 200 rpm shaking. For assays in the presence of stresses, the SIM medium was supplemented with 1% of bile salts, 0.1 mM of H_2O_2, 0.8 M of D-sorbitol, or its pH adjusted to 6, or a combination of the four stresses.

Growth measurements on agar

Strains 17–2, Δ*sci1*, Δ*tssJ*, Δ*clpV,* and *tssB-N3* were grown overnight in SIM medium (three independent cultures/strain) and diluted to an A_{600} of 1. 20 µL were spotted onto 36 disks disposed on SIM agar plates. Upon incubation at 37°C, three disks were recovered at times 2, 3, 4, 5, 6, 7, 8, 9, 10, and 24 h, cells resuspended in 1 mL of SIM and the A_{600} was measured.

Competitive growth measurements on agar

Strains 17–2, Δ*sci1* pTli1, Δ*tssJ*, Δ*clpV*, *tssB-N3*, and Δ*lacZ* were grown overnight in SIM medium (four independent cultures/strain) and diluted to an A_{600} of 1. Two hundred microliters were mixed with 200 µL of the Δ*lacZ* culture. Twenty microliters were spotted onto 15 disks disposed on SIM agar plates. Upon incubation at 37°C, three disks for each mixture were recovered at times 4, 8, and 24 h, cells resuspended in 1 mL of SIM and serially diluted. Triplicates of 100 µL of the 10^{-5} (for 4 h) and 10^{-6} (for 8 h and 24 h) dilutions were spread onto LB-Xgal/IPTG agar plates and incubated at 37°C. The 24 h samples were diluted one-third, and 20 µL were spotted onto three new disks disposed onto a new SIM agar plate and incubated for 24 h (=48 h sample). The last step was repeated twice to yield the 72 and 96 h samples. Blue and white colonies

were counted after ON incubation. For assays in the presence of stresses, the SIM agar was supplemented with 1% of bile salts, 0.1 mM of H_2O_2, 0.8 M of D-sorbitol, or its pH adjusted to 6, or a combination of the four stresses. For all assays, Wilcoxon statistical analyses were performed using the wilcox.test function in R.

SDS-PAGE, western-blotting, imaging, and quantification analyses

Semi-quantitative immunoblotting was performed essentially as previously described (21, 79). Standard methods were used for sodium dodecyl-sulfate polyacrylamide gel electrophoresis (SDS-PAGE) and protein transfer on nitrocellulose membranes. Membranes were probed with anti-His (clone His1, Sigma), and anti-EF-Tu (clone mAb900, HyCult Biotech) monoclonal antibodies, and goat anti-mouse secondary antibodies coupled to AlexaFluor 680 (Invitrogen). Images were recorded at λ = 700 nM using an Odyssey infrared imaging system (LI-COR Bio-sciences). Image analyses were performed with the ImageJ processing program using the Fiji interface (80). Briefly, the image was first converted to grayscale in .jpg format. The rectangle tool of ImageJ was used to select a rectangular area of the size corresponding to the lane width, in order to cover the minimal area to contain the whole of the largest band. The same frame was used to select each Hcp or EF-Tu band. For each selection, the number of pixels was calculated. A control region with no band was also selected to subtract the background. The number of pixels of each band, subtracted from the background, was normalized by dividing by the EF-Tu loading control intensity, to compensate for loading differences. The fold-change relative to the WT strain was then calculated.

Fluorescence microscopy

Cells were grown in SIM medium at 37°C to an A_{600} of 0.6–0.8, resuspended in fresh SIM to an $A_{600\,nm}$ of 10, and 2 µL were spotted onto a thin pad of SIM supplemented with 2% agarose covered with a glass coverslip. Phase contrast and fluorescence were recorded on a Nikon Eclipse Ti2 microscope equipped with a 100 × NA 1.45 Ph3 objective, an Orca-Fusion digital camera (Hamamatsu), and a perfect focus system. All fluorescence images were acquired with a minimal exposure time to minimize bleaching and phototoxicity effects. Exposure times were typically 30 ms for phase contrast and 100 ms for fluorescence channel. Images were analyzed using ImageJ (http://imagej.nih.gov/ij/) and the MicrobeJ v5.11y plugin (81). Statistical dataset analyses were performed with several representative fields from at least three independent biological replicates, using Excel and the R software environment. The number of measured cells or events (*n*) is indicated in each figure.

ACKNOWLEDGMENTS

We thank Etienne Vanlioğlu for construction of the TssB-N3 strains, Jonas Desjardins for designing primers for qRT-PCR analyses, members of the Cascales laboratory for discussions and support, and Moly Ba and Audrey Gozzi for technical support.

This work was funded by the Centre National de la Recherche Scientifique, the Aix-Marseille Université, and by grants from the Agence Nationale de la Recherche (ANR-20-CE11-0017), the Fondation pour la Recherche Médicale (DEQ20180339165), and the Fondation Bettencourt Schueller to E.C. J.F.G. is a recipient of a doctoral fellowship from the French Ministry of Higher Education, Research and Innovation.

B.T. and E.C. designed research. B.T., J.F.G., and E.C. performed research. E.C. wrote the manuscript with contributions from B.T. and J.F.G. All authors contributed to and approved the final revision of the manuscript.

AUTHOR AFFILIATION

[1]Laboratoire d'Ingénierie des Systèmes Macromoléculaires (LISM, UMR 7255), Institut de Microbiologie de la Méditerranée (IMM), Aix Marseille Univ, CNRS, Marseille, France

AUTHOR ORCIDs

Eric Cascales http://orcid.org/0000-0003-0611-9179

AUTHOR CONTRIBUTIONS

Boris Taillefer, Conceptualization, Investigation, Writing – review and editing | Julien F. Giraud, Formal analysis, Investigation, Writing – review and editing | Eric Cascales, Conceptualization, Formal analysis, Funding acquisition, Investigation, Resources, Supervision, Validation, Writing – original draft, Writing – review and editing

DIRECT CONTRIBUTION

This article was submitted via the Active Contributor Track (ACT). Eric Cascales, the ACT-eligible author, secured reviews from Carlos J. Blondel, Universidad Andrés Bello, and Jose A. Bengoechea, Wellcome-Wolfson Institute for Experimental Medicine, Queen's University Belfast.

ADDITIONAL FILES

The following material is available online.

Supplemental Material

Supplemental figures (JB00357-23-s0001.pdf). Figures S1-S4.

REFERENCES

1. Lozupone CA, Stombaugh JI, Gordon JI, Jansson JK, Knight R. 2012. Diversity, stability and resilience of the human gut microbiota. Nature 489:220–230. https://doi.org/10.1038/nature11550
2. de Muinck EJ, Stenseth NC, Sachse D, Vander Roost J, Rønningen KS, Rudi K, Trosvik P. 2013. Context-dependent competition in a model gut bacterial community. PLoS One 8:e67210. https://doi.org/10.1371/journal.pone.0067210
3. Chassaing B, Cascales E. 2018. Antibacterial weapons: targeted destruction in the microbiota. Trends Microbiol 26:329–338. https://doi.org/10.1016/j.tim.2018.01.006
4. Buffie CG, Pamer EG. 2013. Microbiota-mediated colo- nization resistance against intestinal pathogens. Nat Rev Immunol 13:790–801. https://doi.org/10.1038/nri3535
5. Kamada N, Chen GY, Inohara N, Núñez G. 2013. Control of pathogens and pathobionts by the gut microbiota. Nat Immunol 14:685–690. https://doi.org/10.1038/ni.2608
6. Kim S, Covington A, Pamer EG. 2017. The intestinal microbiota: antibiotics, colonization resistance, and enteric pathogens. Immunol Rev 279:90–105. https://doi.org/10.1111/imr.12563
7. Khan I, Bai Y, Zha L, Ullah N, Ullah H, Shah SRH, Sun H, Zhang C. 2021. Mechanism of the gut microbiota colonization resistance and enteric pathogen infection. Front Cell Infect Microbiol 11:716299. https://doi.org/10.3389/fcimb.2021.716299
8. Ghoul M, Mitri S. 2016. The ecology and evolution of microbial competition. Trends Microbiol 24:833–845. https://doi.org/10.1016/j.tim.2016.06.011
9. Granato ET, Meiller-Legrand TA, Foster KR. 2019. The evolution and ecology of bacterial warfare. Curr Biol 29:R521–R537. https://doi.org/10.1016/j.cub.2019.04.024
10. Cascales E, Buchanan SK, Duché D, Kleanthous C, Lloubès R, Postle K, Riley M, Slatin S, Cavard D. 2007. Colicin biology. Microbiol Mol Biol Rev 71:158–229. https://doi.org/10.1128/MMBR.00036-06
11. Kleanthous C. 2010. Swimming against the tide: progress and challenges in our understanding of colicin translocation. Nat Rev Microbiol 8:843–848. https://doi.org/10.1038/nrmicro2454
12. van Kraaij C, de Vos WM, Siezen RJ, Kuipers OP. 1999. Lantibiotics: biosynthesis, mode of action and applications. Nat Prod Rep 16:575–587. https://doi.org/10.1039/a804531c
13. Cenens W, Andrade MO, Llontop E, Alvarez-Martinez CE, Sgro GG, Farah CS. 2020. Bactericidal type IV secretion system homeostasis in *Xanthomonas citri*. PLoS Pathog 16:e1008561. https://doi.org/10.1371/journal.ppat.1008561
14. Ruhe ZC, Low DA, Hayes CS. 2013. Bacterial contact-dependent growth inhibition. Trends Microbiol 21:230–237. https://doi.org/10.1016/j.tim.2013.02.003
15. Zoued A, Brunet YR, Durand E, Aschtgen MS, Logger L, Douzi B, Journet L, Cambillau C, Cascales E. 2014. Architecture and assembly of the type VI secretion system. Biochim Biophys Acta 1843:1664–1673. https://doi.org/10.1016/j.bbamcr.2014.03.018
16. Allsopp LP, Bernal P. 2023. Killing in the name of: T6Ss structure and effector diversity. Microbiology (Reading) 169:001367. https://doi.org/10.1099/mic.0.001367
17. Bowman L, Palmer T. 2021. The type VII secretion system of *Staphylococcus*. Annu Rev Microbiol 75:471–494. https://doi.org/https//doi.org/10.1146/annurev-micro-012721-123600
18. Tran H-KR, Grebenc DW, Klein TA, Whitney JC. 2021. Bacterial type VII secretion: an important player in host-microbe and microbe-microbe interactions. Mol Microbiol 115:478–489. https://doi.org/10.1111/mmi.14680
19. Basler M, Pilhofer M, Henderson GP, Jensen GJ, Mekalanos JJ. 2012. Type VI secretion requires a dynamic contractile phage tail-like structure. Nature 483:182–186. https://doi.org/10.1038/nature10846
20. Basler M. 2015. Type VI secretion system: secretion by a contractile nanomachine. Philos Trans R Soc Lond B Biol Sci 370:20150021. https://doi.org/10.1098/rstb.2015.0021
21. Santin YG, Doan T, Journet L, Cascales E. 2019. Cell width dictates type VI secretion tail length. Curr Biol 29:3707–3713. https://doi.org/10.1016/j.cub.2019.08.058
22. Cascales E. 2017. Microbiology: and amoebophilus invented the machine gun! Curr Biol 27:R1170–R1173. https://doi.org/10.1016/j.cub.2017.09.025
23. Cianfanelli FR, Monlezun L, Coulthurst SJ. 2016. Aim, load, fire: the type VI secretion system, a bacterial nanoweapon. Trends Microbiol 24:51–62. https://doi.org/10.1016/j.tim.2015.10.005

24. Taylor NMI, van Raaij MJ, Leiman PG. 2018. Contractile injection systems of bacteriophages and related systems. Mol Microbiol 108:6–15. https://doi.org/10.1111/mmi.13921
25. Brackmann M, Nazarov S, Wang J, Basler M. 2017. Using force to punch holes: mechanics of contractile nanomachines. Trends Cell Biol 27:623–632. https://doi.org/10.1016/j.tcb.2017.05.003
26. Bingle LE, Bailey CM, Pallen MJ. 2008. Type VI secretion: a beginner's guide. Curr Opin Microbiol 11:3–8. https://doi.org/10.1016/j.mib.2008.01.006
27. Cascales E. 2008. The type VI secretion toolkit. EMBO Rep 9:735–741. https://doi.org/10.1038/embor.2008.131
28. Coyne MJ, Roelofs KG, Comstock LE. 2016. Type VI secretion systems of human gut bacteroidales segregate into three genetic architectures, two of which are contained on mobile genetic elements. BMC Genomics 17:58. https://doi.org/10.1186/s12864-016-2377-z
29. Aschtgen M-S, Bernard CS, De Bentzmann S, Lloubès R, Cascales E. 2008. SciN is an outer membrane lipoprotein required for type VI secretion in enteroaggregative *Escherichia coli*. J Bacteriol 190:7523–7531. https://doi.org/10.1128/JB.00945-08
30. Felisberto-Rodrigues C, Durand E, Aschtgen M-S, Blangy S, Ortiz-Lombardia M, Douzi B, Cambillau C, Cascales E. 2011. Towards a structural comprehension of bacterial type VI secretion systems: characterization of the TssJ-TssM complex of an *Escherichia coli* pathovar. PLoS Pathog 7:e1002386. https://doi.org/10.1371/journal.ppat.1002386
31. Durand E, Nguyen VS, Zoued A, Logger L, Péhau-Arnaudet G, Aschtgen MS, Spinelli S, Desmyter A, Bardiaux B, Dujeancourt A, Roussel A, Cambillau C, Cascales E, Fronzes R. 2015. Biogenesis and structure of a type VI secretion membrane core complex. Nature 523:555–560. https://doi.org/10.1038/nature14667
32. Rapisarda C, Cherrak Y, Kooger R, Schmidt V, Pellarin R, Logger L, Cascales E, Pilhofer M, Durand E, Fronzes R. 2019. *In situ* and high-resolution cryo-EM structure of a bacterial type VI secretion system membrane complex. EMBO J 38:e100886. https://doi.org/10.15252/embj.2018100886
33. Zoued A, Durand E, Bebeacua C, Brunet YR, Douzi B, Cambillau C, Cascales E, Journet L. 2013. TssK is a Trimeric cytoplasmic protein interacting with components of both phage-like and membrane anchoring complexes of the type VI secretion system. J Biol Chem 288:27031–27041. https://doi.org/10.1074/jbc.M113.499772
34. Nguyen VS, Logger L, Spinelli S, Legrand P, Huyen Pham TT, Nhung Trinh TT, Cherrak Y, Zoued A, Desmyter A, Durand E, Roussel A, Kellenberger C, Cascales E, Cambillau C. 2017. Type VI secretion TssK baseplate protein exhibits structural similarity with phage receptor-binding proteins and evolved to bind the membrane complex. Nat Microbiol 2:17103. https://doi.org/10.1038/nmicrobiol.2017.103
35. Vanlioğlu E, Santin YG, Filella-Merce I, Pellarin R, Cascales E. 2023. Coevolution-guided mapping of the type VI secretion membrane complex-baseplate interface. J Mol Biol 435:167918. https://doi.org/10.1016/j.jmb.2022.167918
36. Shneider MM, Buth SA, Ho BT, Basler M, Mekalanos JJ, Leiman PG. 2013. PAAR-repeat proteins sharpen and diversify the type VI secretion system spike. Nature 500:350–353. https://doi.org/10.1038/nature12453
37. English G, Byron O, Cianfanelli FR, Prescott AR, Coulthurst SJ. 2014. Biochemical analysis of TssK, a core component of the bacterial type VI secretion system, reveals distinct oligomeric states of TssK and identifies a TssK-TssFG subcomplex. Biochem J 461:291–304. https://doi.org/10.1042/BJ20131426
38. Nazarov S, Schneider JP, Brackmann M, Goldie KN, Stahlberg H, Basler M. 2018. Cryo-EM reconstruction of type VI secretion system baseplate and sheath distal end. EMBO J 37:e97103. https://doi.org/10.15252/embj.201797103
39. Cherrak Y, Rapisarda C, Pellarin R, Bouvier G, Bardiaux B, Allain F, Malosse C, Rey M, Chamot-Rooke J, Cascales E, Fronzes R, Durand E. 2018. Biogenesis and structure of a type VI secretion baseplate. Nat Microbiol 3:1404–1416. https://doi.org/10.1038/s41564-018-0260-1
40. Bönemann G, Pietrosiuk A, Diemand A, Zentgraf H, Mogk A. 2009. Remodelling of VipA/VipB tubules by ClpV-mediated threading is crucial for type VI protein secretion. EMBO J 28:315–325. https://doi.org/10.1038/emboj.2008.269
41. Pietrosiuk A, Lenherr ED, Falk S, Bönemann G, Kopp J, Zentgraf H, Sinning I, Mogk A. 2011. Molecular basis for the unique role of the AAA+ chaperone ClpV in type VI protein secretion. J Biol Chem 286:30010–30021. https://doi.org/10.1074/jbc.M111.253377
42. Kapitein N, Bönemann G, Pietrosiuk A, Seyffer F, Hausser I, Locker JK, Mogk A. 2013. ClpV recycles VipA/VipB tubules and prevents non-productive tubule formation to ensure efficient type VI protein secretion. Mol Microbiol 87:1013–1028. https://doi.org/10.1111/mmi.12147
43. Unni R, Pintor KL, Diepold A, Unterweger D. 2022. Presence and absence of type VI secretion systems in bacteria. Microbiology (Reading) 168. https://doi.org/10.1099/mic.0.001151
44. Lin YL, Smith SN, Kanso E, Septer AN, Rycroft CH. 2023. A subcellular biochemical model for T6SS dynamics reveals winning competitive strategies. PNAS Nexus 2:gad195. https://doi.org/10.1093/pnasnexus/pgad195
45. Gupta S, Ray S, Khan A, China A, Das D, Mallick AI. 2021. The cost of bacterial predation via type VI secretion system leads to predator extinction under environmental stress. iScience 24:103507. https://doi.org/10.1016/j.isci.2021.103507
46. Robitaille S, Simmons EL, Verster AJ, McClure EA, Royce DB, Trus E, Swartz K, Schultz D, Nadell CD, Ross BD. 2023. Community composition and the environment modulate the population dynamics of type VI secretion in human gut bacteria. Nat Ecol Evol. https://doi.org/10.1038/s41559-023-02230-6
47. Septer AN, Sharpe G, Shook EA. 2023. The *Vibrio fischeri* type VI secretion system incurs a fitness cost under host-like conditions. bioRxiv:2023.03.07.529561. https://doi.org/10.1101/2023.03.07.529561
48. Zhang C, Ratcliff WC, Hammer BK. 2023. Constitutive expression of the type VI secretion system carries no measurable fitness cost in Vibrio Cholerae. bioRxiv:2023.03.24.534098. https://doi.org/10.1101/2023.03.24.534098
49. Yin M, Yan Z, Li X. 2019. Architecture of type VI secretion system membrane core complex. Cell Res 29:251–253. https://doi.org/10.1038/s41422-018-0130-7
50. Wang J, Brackmann M, Castaño-Díez D, Kudryashev M, Goldie KN, Maier T, Stahlberg H, Basler M. 2017. Cryo-EM structure of the extended type VI secretion system sheath-tube complex. Nat Microbiol 2:1507–1512. https://doi.org/10.1038/s41564-017-0020-7
51. Brackmann M, Wang J, Basler M. 2018. Type VI secretion system sheath inter-subunit interactions modulate its contraction. EMBO Rep 19:225–233. https://doi.org/10.15252/embr.201744416
52. Bönemann G, Pietrosiuk A, Mogk A. 2010. Tubules and donuts: a type VI secretion story. Mol Microbiol 76:815–821. https://doi.org/10.1111/j.1365-2958.2010.07171.x
53. Förster A, Planamente S, Manoli E, Lossi NS, Freemont PS, Filloux A. 2014. Coevolution of the ATPase ClpV, the sheath proteins TssB and TssC, and the accessory protein TagJ/HsiE1 distinguishes type VI secretion classes. J Biol Chem 289:33032–33043. https://doi.org/10.1074/jbc.M114.600510
54. Douzi B, Brunet YR, Spinelli S, Lensi V, Legrand P, Blangy S, Kumar A, Journet L, Cascales E, Cambillau C. 2016. Structure and specificity of the type VI secretion system ClpV-TssC interaction in enteroaggregative *Escherichia coli*. Sci Rep 6:34405. https://doi.org/10.1038/srep34405
55. Brunet YR, Bernard CS, Gavioli M, Lloubès R, Cascales E. 2011. An epigenetic switch involving overlapping fur and DNA methylation optimizes expression of a type VI secretion gene cluster. PLoS Genet 7:e1002205. https://doi.org/10.1371/journal.pgen.1002205
56. Dawson PA. 1998. Bile secretion and the enterohepatic circulation of bile acids, p 1052–1063. In Feldman M, MH Sleisenger, BF Scharschmidt (ed), Sleisenger and fordtran's gastrointestinal and liver disease: pathophysiology/diagnosis/management, 6th ed. W. B. Saunders, Co, Philadelphia, PA.
57. Rojas E, Theriot JA, Huang KC. 2014. Response of *Escherichia coli* growth rate to osmotic shock. Proc Natl Acad Sci U S A 111:7807–7812. https://doi.org/10.1073/pnas.1402591111
58. Rodríguez-Rojas A, Kim JJ, Johnston PR, Makarova O, Eravci M, Weise C, Hengge R, Rolff J. 2020. Non-lethal exposure to H_2O_2 boosts bacterial survival and evolvability against oxidative stress. PLoS Genet 16:e1008649. https://doi.org/10.1371/journal.pgen.1008649
59. Fallingborg J. 1999. Intraluminal pH of the human gastrointestinal tract. Dan Med Bull 46:183–196.

60. Brunet YR, Espinosa L, Harchouni S, Mignot T, Cascales E. 2013. Imaging type VI secretion-mediated bacterial killing. Cell Rep 3:36–41. https://doi.org/10.1016/j.celrep.2012.11.027
61. Flaugnatti N, Le TTH, Canaan S, Aschtgen M-S, Nguyen VS, Blangy S, Kellenberger C, Roussel A, Cambillau C, Cascales E, Journet L. 2016. A phospholipase A1 antibacterial type VI secretion effector interacts directly with the C-terminal domain of the VgrG spike protein for delivery. Mol Microbiol 99:1099–1118. https://doi.org/10.1111/mmi.13292
62. Hibbing ME, Fuqua C, Parsek MR, Peterson SB. 2010. Bacterial competition: surviving and thriving in the microbial jungle. Nat Rev Microbiol 8:15–25. https://doi.org/10.1038/nrmicro2259
63. Sana TG, Flaugnatti N, Lugo KA, Lam LH, Jacobson A, Baylot V, Durand E, Journet L, Cascales E, Monack DM. 2016. *Salmonella typhimurium* utilizes a T6SS-mediated antibacterial weapon to establish in the host gut. Proc Natl Acad Sci U S A 113:E5044–51. https://doi.org/10.1073/pnas.1608858113
64. Wexler AG, Bao Y, Whitney JC, Bobay LM, Xavier JB, Schofield WB, Barry NA, Russell AB, Tran BQ, Goo YA, Goodlett DR, Ochman H, Mougous JD, Goodman AL. 2016. Human symbionts inject and neutralize antibacterial toxins to persist in the gut. Proc Natl Acad Sci U S A 113:3639–3644. https://doi.org/10.1073/pnas.1525637113
65. Chatzidaki-Livanis M, Geva-Zatorsky N, Comstock LE. 2016. Bacteroides fragilis type VI secretion systems use novel effector and immunity proteins to antagonize human gut bacteroidales species. Proc Natl Acad Sci U S A 113:3627–3632. https://doi.org/10.1073/pnas.1522510113
66. Hecht AL, Casterline BW, Earley ZM, Goo YA, Goodlett DR, Bubeck Wardenburg J. 2016. Strain competition restricts colonization of an enteric pathogen and prevents colitis. EMBO Rep 17:1281–1291. https://doi.org/10.15252/embr.201642282
67. Anderson MC, Vonaesch P, Saffarian A, Marteyn BS, Sansonetti PJ. 2017. *Shigella sonnei* encodes a functional T6SS used for interbacterial competition and niche occupancy. Cell Host Microbe 21:769–776. https://doi.org/10.1016/j.chom.2017.05.004
68. Logan SL, Thomas J, Yan J, Baker RP, Shields DS, Xavier JB, Hammer BK, Parthasarathy R. 2018. The *Vibrio cholerae* type VI secretion system can modulate host intestinal mechanics to displace gut bacterial Symbionts. Proc Natl Acad Sci U S A 115:E3779–E3787. https://doi.org/10.1073/pnas.1720133115
69. Zhao W, Caro F, Robins W, Mekalanos JJ. 2018. Antagonism toward the intestinal microbiota and its effect on *Vibrio cholerae* virulence. Science 359:210–213. https://doi.org/10.1126/science.aap8775
70. Calderon-Gonzalez R, Lee A, Lopez-Campos G, Hancock SJ, Sa-Pessoa J, Dumigan A, McMullan R, Campbell EL, Bengoechea JA. 2023. Modelling the gastrointestinal carriage of *Klebsiella pneumoniae* infections. mBio 14:e0312122. https://doi.org/10.1128/mbio.03121-22
71. Milo R. 2013. What is the total number of protein molecules per cell volume? a call to rethink some published values. Bioessays 35:1050–1055. https://doi.org/10.1002/bies.201300066
72. Lynch M, Marinov GK. 2015. The bioenergetic costs of a gene. Proc Natl Acad Sci U S A 112:15690–15695. https://doi.org/10.1073/pnas.1514974112
73. Sauer RT, Bolon DN, Burton BM, Burton RE, Flynn JM, Grant RA, Hersch GL, Joshi SA, Kenniston JA, Levchenko I, Neher SB, Oakes ESC, Siddiqui SM, Wah DA, Baker TA. 2004. Sculpting the proteome with AAA(+) proteases and disassembly machines. Cell 119:9–18. https://doi.org/10.1016/j.cell.2004.09.020
74. Lowry OH, Carter J, Ward JB, Glaser L. 1971. The effect of carbon and nitrogen sources on the level of metabolic intermediates in *Escherichia coli*. J Biol Chem 246:6511–6521.
75. Sturm A, Heinemann M, Arnoldini M, Benecke A, Ackermann M, Benz M, Dormann J, Hardt W-D. 2011. The cost of virulence: retarded growth of *Salmonella typhimurium* cells expressing type III secretion system 1. PLoS Pathog 7:e1002143. https://doi.org/10.1371/journal.ppat.1002143
76. Link AJ, Phillips D, Church GM. 1997. Methods for generating precise deletions and insertions in the genome of wild-type *Escherichia coli*: application to open reading frame characterization. J Bacteriol 179:6228–6237. https://doi.org/10.1128/jb.179.20.6228-6237.1997
77. Datsenko KA, Wanner BL. 2000. One-step inactivation of chromosomal genes in *Escherichia coli* K-12 using PCR products. Proc Natl Acad Sci U S A 97:6640–6645. https://doi.org/10.1073/pnas.120163297
78. Chaveroche MK, Ghigo JM, d'Enfert C. 2000. A rapid method for efficient gene replacement in the filamentous fungus *Aspergillus nidulans*. Nucleic Acids Res 28:E97. https://doi.org/10.1093/nar/28.22.e97
79. Zoued A, Duneau JP, Durand E, España AP, Journet L, Guerlesquin F, Cascales E. 2018. Tryptophan-mediated dimerization of the TssL transmembrane anchor is required for type VI secretion system activity. J Mol Biol 430:987–1003. https://doi.org/10.1016/j.jmb.2018.02.008
80. Schindelin J, Arganda-Carreras I, Frise E, Kaynig V, Longair M, Pietzsch T, Preibisch S, Rueden C, Saalfeld S, Schmid B, Tinevez JY, White DJ, Hartenstein V, Eliceiri K, Tomancak P, Cardona A. 2012. Fiji: an open-source platform for biological-image analysis. Nat Methods 9:676–682. https://doi.org/10.1038/nmeth.2019
81. Ducret A, Quardokus EM, Brun YV. 2016. MicrobeJ, a tool for high throughput bacterial cell detection and quantitative analysis. Nat Microbiol 1:16077. https://doi.org/10.1038/nmicrobiol.2016.77

Supplemental Information

No fitness cost entailed by type VI secretion synthesis, assembly, contraction or disassembly in enteroaggregative *Escherichia coli.*

Boris Taillefer, Julien F. Giraud, and Eric Cascales

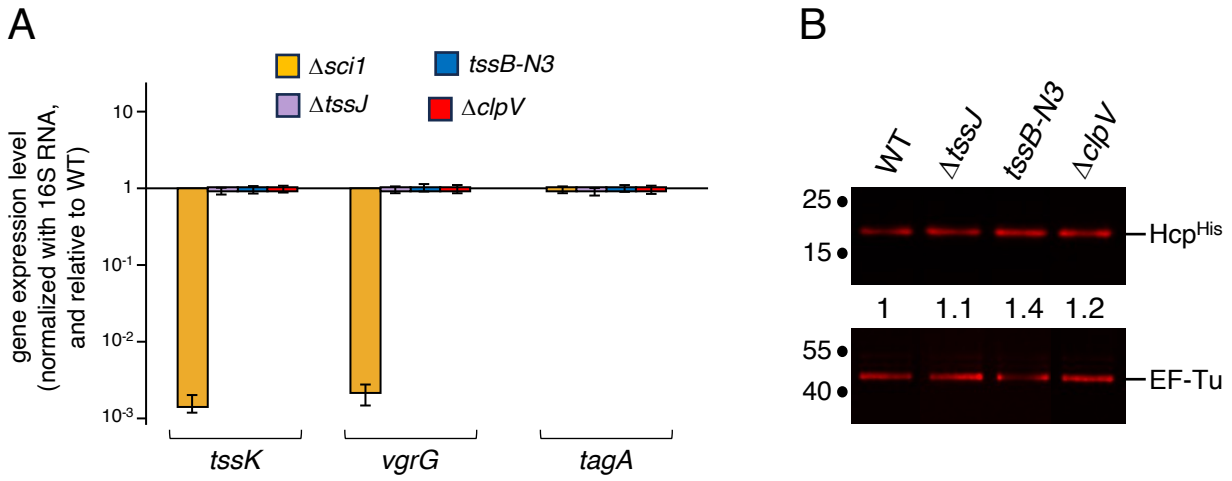

Supplemental Figure 1 | T6SS gene expression and Hcp production in EAEC mutant strains used in this work. (A) qRT-PCR analyses of the T6SS *sci1 tssK*, *vgrG* and *tagA* gene. The expression levels were normalized to the 16S RNA levels are presented relative to the wild-type strain. (B) Western blot analyses of Hcp abundance. The total cell extracts of 4×108 cells of the indicated strain producing 6×His-tagged Hcp (Hcp^{His}) were subjected to 12.5% acrylamide SDS- PAGE and immunodetected with anti-His (upper panel) and -EF-Tu (lower panel) monoclonal primary antibodies and secondary antibodies coupled to Alexa Fluor 680. The Hcp levels, normalized to the EF-Tu levels (loading control) are presented relative to the wild-type strain (under the Hcp blot). Molecular weight markers (in kDa) are indicated on the left.

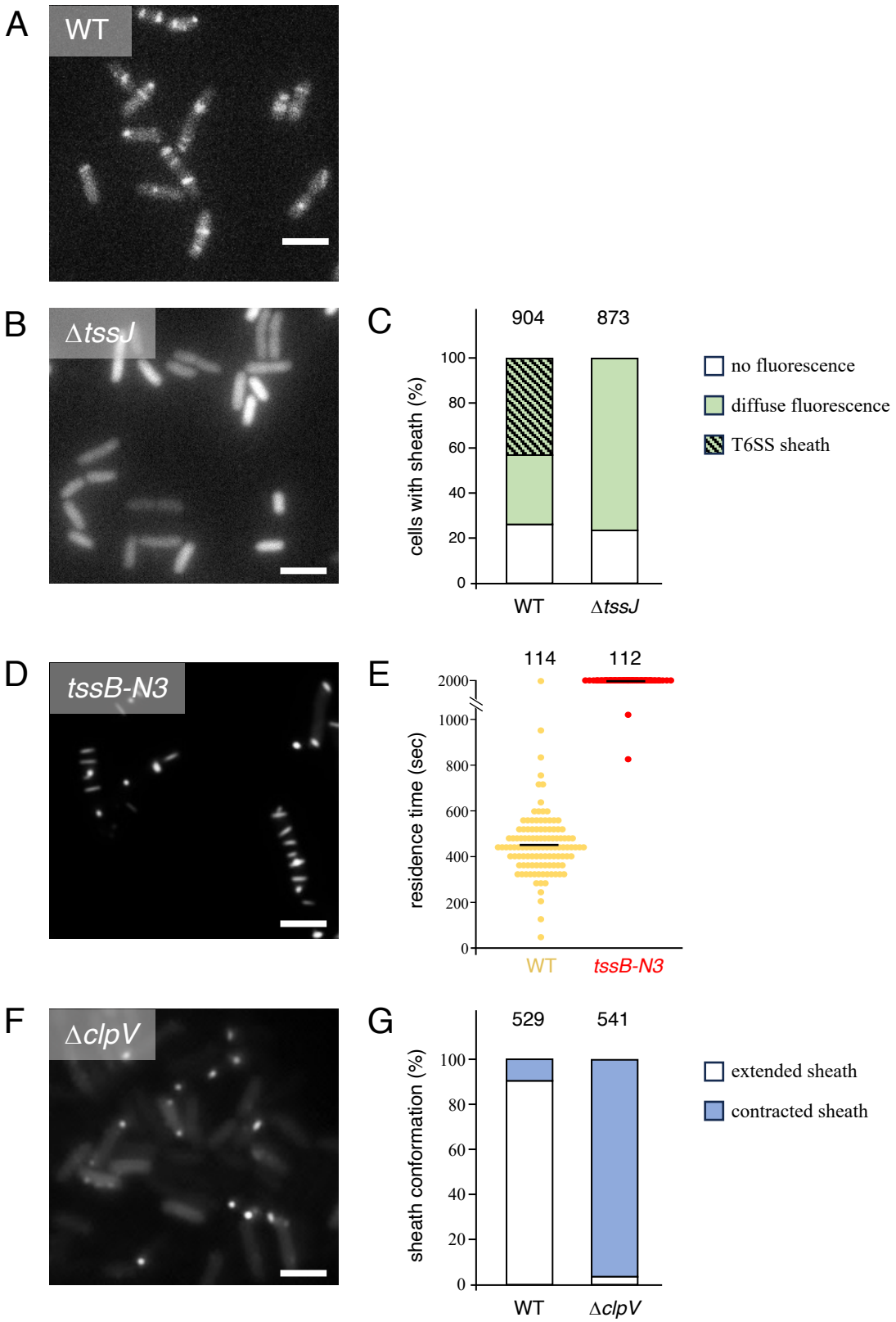

Supplemental Figure 2 | T6SS phenotypes associated with EAEC mutant strains used in this work. Representative fields of fluorescence microscopy recordings of the WT (A), Δ*tssJ* (B), *tssB-N3* (D) and Δ*clpV* (F) strains expressing a chromosomal *tssB-sfGFP* fusion. Scale bar, 2 µm. (C) T6SS sheath assembly in WT and Δ*tssJ* cells expressing the chromosomal *tssB-sfGFP* fusion. Cells with no fluorescence (*i.e.*, that do not express the T6SS), with diffuse fluorescence (*i.e.*, that express but do not assemble the T6SS) and with tubular structures (*i.e.*, that assemble the T6SS) are shown in white, green, and stripped green, respectively. The number of cells analyzed for each strain (*n*) is indicated on top. (E) Sheath residence time in WT (orange) and *tssB-N3* mutant (red) cells (horizontal bar, mean average). The number of analyzed sheath assembly/contraction events (*n*) is indicated on top. Data acquisition has been done for 2,000 sec. (G) T6SS sheath disassembly in WT and Δ*clpV* cells expressing the chromosomal *tssB-sfGFP* fusion. The percentage of extended and contracted sheaths are shown in white and blue, respectively. The number of cells analyzed for each strain (*n*) is indicated on top.

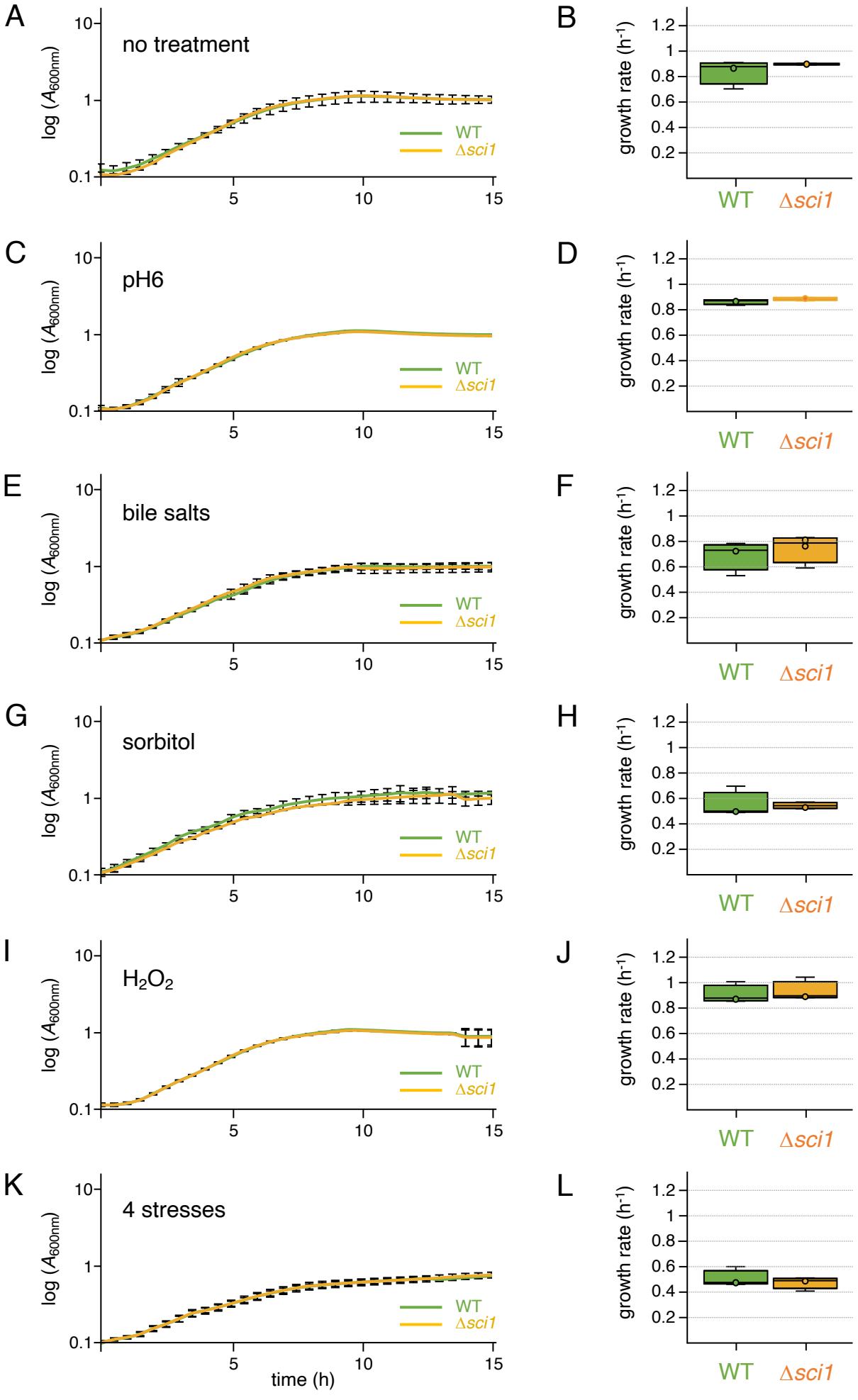
A
no treatment
log (A_{600nm})
WT
Δsci1
B
growth rate (h^{-1})
WT
Δsci1
C
pH6
D
E
bile salts
F
G
sorbitol
H
I
H_2O_2
J
K
4 stresses
L
time (h)

Supplemental Figure 3 | Growth of T6SS mutant strains in the presence of various stresses. (A, C, E, G, I, K) 15-hour growth curves of the wild-type (WT) and Δ*sci1* strains grown in SIM medium in the presence of the indicated stress (A, no stress; C, pH6; E, 1% of bile salts; G, 0.8 M of sorbitol; I, 0.1 mM of H_2O_2; K, combination of the four stresses). The values represent the average and standard deviation from 8 measures (4 biological replicates, 2 independent measures/replicate). (B, D, F, H, J, L) Box-and-whisker representation (horizontal bar, median value; lower and upper boundaries of the box plot, 25% and 75% percentiles, respectively; whiskers, 10% and 90% percentiles) of the growth rates of the WT and Δ*sci1* strains in SIM medium in the presence of the indicated stress (B, no stress; D, pH6; F, 1% of bile salts; H, 0.8 M of sorbitol; J, 0.1 mM of H_2O_2; L, combination of the four stresses).

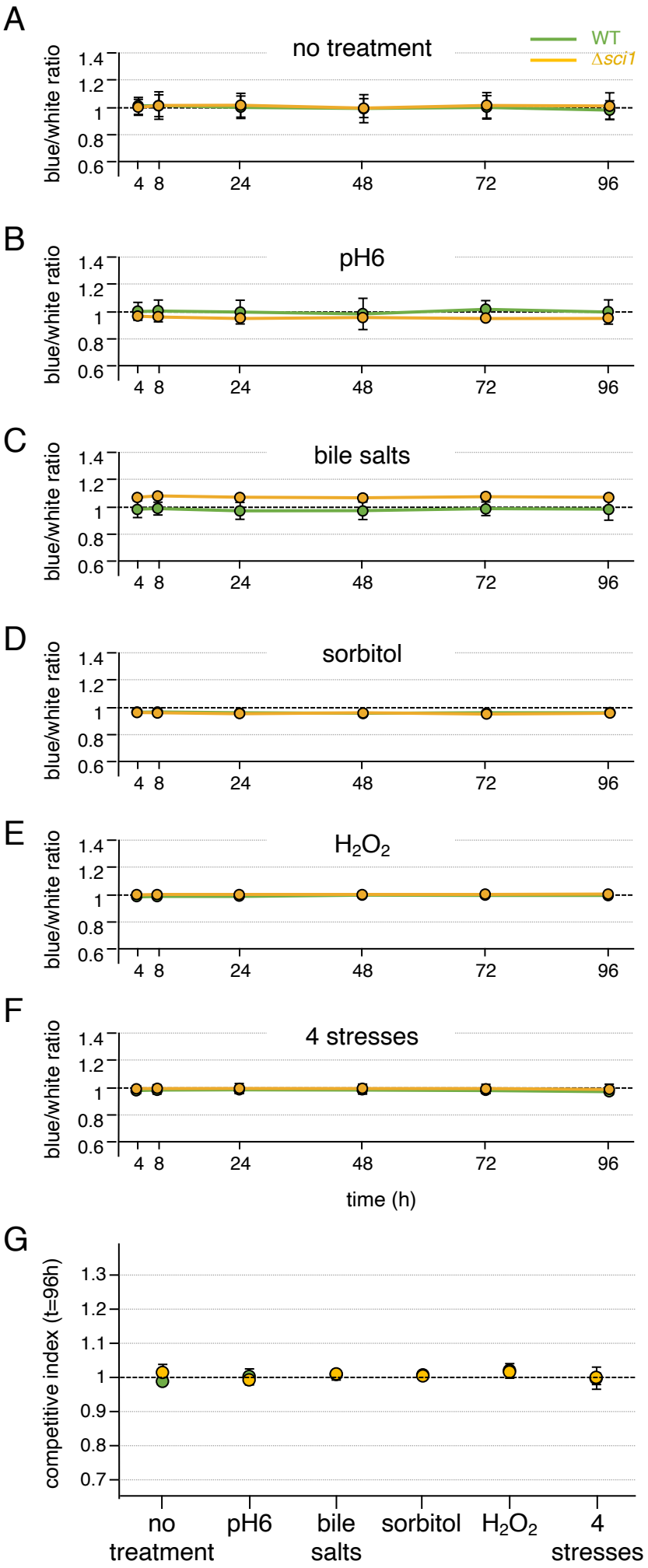
A
no treatment
WT
Δsci1
blue/white ratio
1.4
1.2
1
0.8
0.6
4 8 24 48 72 96
B
pH6
C
bile salts
D
sorbitol
E
H2O2
F
4 stresses
time (h)
G
competitive index (t=96h)
1.3
1.2
1.1
1
0.9
0.8
0.7
no treatment
pH6
bile salts
sorbitol
H2O2
4 stresses

Supplemental Figure 4 | A T6SS mutant does not outcompete the wild-type strain in the presence of various stresses. (A-F) Variation of the ratio of WT (green) or Δ*sci1* (orange) strains versus 17-2Δ*lacZ* over time grown in SIM agar in the presence of the indicated stress (A, no treatment; B, pH6; C, 1% of bile salts; D, 0.8 M of sorbitol; E, 0.1 mM of H_2O_2; F, combination of the four stresses). The values represent the average of 2 biological replicates. (G) Competitive indexes of WT (green) or Δ*sci1* (orange) strains versus 17-2Δ*lacZ* (WT/Δ*lacZ* or Δ*sci1*/Δ*lacZ* ratio after 96h of co-culture divided by the initial ratio) in the presence of the indicated stress. The values represent the average of 2 biological replicates.